

# Numerical Simulations of the Diameter Effect for Nitromethane Using Ignition and Growth Model

Yuta Sugiyama, Kunihiko Wakabayashi, Tomoharu Matsumura, Yoshio Nakayama  
National Institute of Advanced Industrial Science and Technology  
Tsukuba, Ibaraki, Japan

## 1 Introduction

Detonations are supersonic flow phenomena with leading shock waves that ignite high explosives. When the high explosives is accidentally detonated, the shock pressure becomes in the range of 10 GPa, and the generated blast wave and the fragments are hazard to people and have the potential to cause extensive damage to inhabited area. In order to store and use the high explosives safely, the explosive properties such as shock initiation and diameter effect should be clarified and are investigated by many researchers using experimental, theoretical, and numerical approaches. Detonation velocity of infinite diameter charge such as RDX, TNT and PETN agrees well with the Zeldovich, von Neumann and Döring (ZND) model. However, as the diameter decreases, radial flows will curve the detonation front, and chemical reaction near the interface between explosives and surrounding material is inhibited. When the diameter becomes small, the detonation velocity decreases. Below the critical diameter, detonations do not maintain its propagation. Campbell and Engelke [1] showed the dependence of steady detonation velocity on charge diameter of several explosives in cylindrical configuration and gave fitting formulas that fit experimental data. In order to estimate the detonation properties, Petitpas *et al.* [2] and Schoch *et al.* [3] developed a hyperbolic multiphase flow model with a single pressure and a single velocity but different temperatures between fluids. They used stiffened gas and Jones-Wilkins-Lee (JWL) equations of state, and a single step chemical reaction model.

The objective of this study is to simulate the behavior of detonation propagation by using a numerical model by Petitpas *et al.*[2] and Schoch *et al.*[3] in order to estimate the hazard assessment of the high explosives. In the present paper, nitromethane (NM) is used for the high explosive, and the parameter is the diameter of cylindrical NM to discuss the diameter effect and critical diameter in the case of the light and heavy confinements.

## 2 Numerical method

The single-pressure and single-velocity multi-phase model (1), (2) and (4), proposed by Petitpas *et al.* [2] and Schoch *et al.* [3], is used in the present study. The details of the numerical algorithm are described in Refs. [2] and [3], and the model, which contains following three steps to solve the detonation propagation, are summarized.

- 1) Hyperbolic step: the pressure non-equilibrium model is advanced in time. The convective term is discretized using the third-order Harten-Lax-van Leer for contact (HLLC) scheme [4] by monotonic upstream-centered scheme for conservation laws (MUSCL) interpolation with a linear scaling limiter [5]. The three-stage TVD Runge–Kutta method [6] is used for time integrations of the hyperbolic step.

$$\left\{ \begin{array}{l} \frac{\partial \alpha_i}{\partial t} + \mathbf{u} \cdot \bar{\nabla} \alpha_i = 0 \\ \frac{\partial \rho_i \alpha_i}{\partial t} + \text{div}(\rho_i \alpha_i \mathbf{u}) = -\frac{\rho_i \alpha_i u_y}{y} \\ \frac{\partial \rho \mathbf{u}}{\partial t} + \text{div}(\rho \mathbf{u} \otimes \mathbf{u}) = -\frac{\rho u_y}{y} \mathbf{u} \\ \frac{\partial \rho_i \alpha_i \varepsilon_i}{\partial t} + \text{div}(\rho_i \alpha_i \varepsilon_i \mathbf{u}) + \alpha_i p_i \text{div}(\mathbf{u}) = -\frac{\alpha_i (\rho_i \varepsilon_i + p_i) u_y}{y} \\ \frac{\partial \rho E}{\partial t} + \text{div}((\rho E + p) \mathbf{u}) = -\frac{(\rho E + p) u_y}{y} \end{array} \right. \quad (1)$$

where,  $\rho = \sum_i \rho_i \alpha_i$ ,  $p = \sum_i p_i \alpha_i$

- 2) Pressure relaxation step: After hyperbolic step, internal energies  $\varepsilon_i$  estimate pressures, which are non-equilibrium. Solving the ordinary differential equation (2) with the Newton-Raphson method [7] achieves the pressure equilibrium condition ( $p' = p_i$ ) and the corrected volume fraction  $\alpha_i^*$  and density  $\rho_i^*$  of  $i$ -th fluid. Here  $\mu$  tends to infinity, and  $P_1$  denotes the interfacial pressure. In this step, mass ( $\rho_i \alpha_i$ ), momentum ( $\rho \mathbf{u}$ ) and total energy ( $\rho E$ ) are assumed to be constant. Since the internal energy equation in Eq. (1) is non-conservative, the relaxed pressure should be re-estimated by the conservative values. After determination of corrected volume fraction  $\alpha_i^*$  and density  $\rho_i^*$ , the mixture equation of state (3) gives the equilibrium pressure.

$$\left\{ \begin{array}{l} \frac{\partial \alpha_i}{\partial t} = \mu (p' - p_i) \\ \frac{\partial \rho_i \alpha_i \varepsilon_i}{\partial t} = p_i \mu (p' - p_i) \end{array} \right. \quad (2)$$

$$\rho E - \frac{1}{2} \rho \mathbf{u} \cdot \mathbf{u} = \sum_i \alpha_i^* \rho_i^* \varepsilon_i \quad (3)$$

- 3) Chemical reaction step: Chemical reaction is progressed by solving the ordinary differential equation (4) under pressure equilibrium condition. The three-stage TVD Runge–Kutta method [6] is used for time integrations of the chemical reaction step.

$$\left\{ \begin{array}{l} \frac{\partial \alpha_i}{\partial t} = \frac{\rho r_i}{\rho_i} - \frac{\alpha_i}{\rho_i c_i^2} \rho c^2 \sum_j \frac{\rho r_j}{\rho_j} \\ \frac{\partial \rho_i \alpha_i}{\partial t} = \rho r_i \end{array} \right. \quad (4)$$

$\rho_i$ ,  $\alpha_i$ ,  $p_i$ ,  $c_i$ ,  $r_i$  and  $\varepsilon_i$  are the density, volume fraction, pressure, sound speed, reaction rate (described later) and internal energy of  $i$ -th fluid, respectively.  $\rho$ ,  $p$ ,  $c$  and  $E$  denote the total density, mixture pressure, mixture sound speed and the total energy,  $\mathbf{u}$  is the velocity vector of  $(u_x, u_y)$  in  $x$  and  $y$

directions. Four fluids are modeled by equations of state of JWL [8-10] (5) for the unreacted NM and of JWL (6) for the detonation products, of ideal gas for air (7) as a light confinement and of stiffened gas (8) for brass as a heavy confinement, respectively. Mixture sound speed  $c$  is estimated by Eq. (9).

$$\frac{\varepsilon_1}{v_{01}} = \frac{p_1 v_1^*}{\omega_1} - f_1(v_1^*) + f_1(1) + \frac{Q_1}{v_{01}} \quad (5)$$

$$\text{where, } f_1(v_1^*) = A_1 \left( \frac{v_1^*}{\omega_1} - \frac{1}{R_{11}} \right) \exp(-R_{11} v_1^*) + B_1 \left( \frac{v_1^*}{\omega_1} - \frac{1}{R_{21}} \right) \exp(-R_{21} v_1^*), \quad v_1^* = \frac{v_1}{v_{01}}$$

$$\frac{\varepsilon_2}{v_{01}} = \frac{p_2 v_2^*}{\omega_2} - f_2(v_2^*) + \frac{Q_2}{v_{01}} \quad (6)$$

$$\text{where, } f_2(v_2^*) = A_2 \left( \frac{v_2^*}{\omega_2} - \frac{1}{R_{12}} \right) \exp(-R_{12} v_2^*) + B_2 \left( \frac{v_2^*}{\omega_2} - \frac{1}{R_{22}} \right) \exp(-R_{22} v_2^*), \quad v_2^* = \frac{v_2}{v_{01}}$$

$$\varepsilon_3 = \frac{p_3}{(\gamma_3 - 1)\rho_3} \quad (7)$$

$$\varepsilon_4 = \frac{p_4 + \gamma_4 \pi}{(\gamma_4 - 1)\rho_4} \quad (8)$$

$$\rho c^2 = \sum \rho_i c_i^2 \quad (9)$$

$$\text{where } c_i^2 = \left( \frac{\partial p_i}{\partial \rho_i} \right)_{\varepsilon_i} + \frac{p_i}{\rho_i^2} \left( \frac{\partial p_i}{\partial \varepsilon_i} \right)_{\rho_i}$$

$v_{01}$  indicates the initial specific volume of the explosive ( $1/\rho_0$ ).  $v_i^*$  and  $v_i$  are the relative volume and the specific volume, respectively.  $Q_i$  and  $\omega_i$  denote the heat release and Grüneisen coefficient.  $A_i$ ,  $B_i$ ,  $R_{1i}$  and  $R_{2i}$  are constants depending on the explosive. In the present study, we model unreacted NM, detonation products, air and brass. Unreacted NM and detonation products are modeled by the JWL equations of state, and ignition and growth model [12] is used for the chemical reaction. The parameters for NM are described in Table 1 [11]. The parameters of equations of state for air and brass are  $\gamma_3 = 1.4$ ,  $\gamma_4 = 3.75$  and  $\pi = 3.24 \times 10^{10}$ .

Table 1 JWL parameters for nitromethane [11]

Nitromethane ( $\rho_0 = 1137 \text{ kg/m}^3$ )			
Unreacted ( $i = 1$ )		Product ( $i = 2$ )	
$A_1$	30 Mbar	$A_2$	2.092 Mbar
$B_1$	-0.018003 Mbar	$B_2$	0.05689 Mbar
$R_{11}$	10	$R_{12}$	4.4
$R_{21}$	1	$R_{22}$	1.2
$\omega_1$	1.237	$\omega_2$	0.3
$Q_1$	4.52 MJ/kg	$Q_2$	0 MJ/kg

$$\begin{aligned} r_2 = -r_1 &= I(1-\lambda)^b \left( \frac{1}{v^*} - 1 - a \right)^x & (\lambda < \lambda_{ig,\max}) \\ &+ G_1(1-\lambda)^c \lambda^d P^y & (0 < \lambda < \lambda_{G1,\max}) \\ &+ G_2(1-\lambda)^e \lambda^g P^z & (\lambda_{G2,\min} < \lambda) \end{aligned} \quad (10)$$

In order to estimate the explosive properties, we use the ignition and growth model developed by Lee and Tarver [12] as shown in Eq. (10) to simulate the detonation propagation of condensed explosives.

Here,  $\lambda$  and  $P$  are the mass fraction of product and pressure in Mbar, respectively.  $\lambda_{ig,max}$ ,  $\lambda_{G1,max}$  and  $\lambda_{G2,min}$  are the mass fractions at which the three terms are activated. The first term models the hot spot formation, where a small fraction of explosive is ignited. The second term is a growth term for the spread of hot spots into the bulk of the explosives, and the third term models the later times of the reaction.  $a, b, c, d, e, g, x, y, z, I, G_1$  and  $G_2$  are constants to describe the proper chemical reaction rate depending on the explosive listed in Table 2 [11].

Figure 1 shows a schematic diagram of the calculation target and the initial condition of the explosive. Here,  $d$  denotes the diameter of the cylindrical explosive and is a parameter in the present study. Symmetric axis is located at  $y = 0$ . At ignition point, we put high-pressure detonation products that can instantaneously generate the overdriven detonation at the interface between explosive and ignition region. Table 3 shows the calculation cases in the present study. We model NM surrounded by the brass or by the air to discuss the diameter effect of the different confinement. At the inert material, air of  $1.2 \text{ kg/m}^3$  or brass of  $8450 \text{ kg/m}^3$  is set. Figure 2 shows results of 1D steady analysis of CJ detonation wave. In the present study, CJ detonation velocity and CJ pressure are  $6240 \text{ m/s}$  and  $12.5 \text{ GPa}$ , respectively, and agree well with the previous numerical data[13]. The first two reaction length is around  $80 \text{ }\mu\text{m}$ . We simulated the diameter effect with  $5 \text{ }\mu\text{m}$  grid resolution and confirmed that the diameter effect does not depend on the grid resolution. Then, we believed that  $10 \text{ }\mu\text{m}$  grid resolution is enough to solve the detonation propagation of NM, and the constant grid spacing of  $10 \text{ }\mu\text{m}$  set in all regions.

Table 2 Reaction parameters

	Nitromethane	unit
$I$	1000	$\mu\text{s}^{-1}$
$a$	0.5741	-
$b$	0.667	-
$x$	4	-
$\lambda_{ig,max}$	0.01	-
$G_1$	121875	$\text{Mbar}^{-y} \mu\text{s}^{-1}$
$c$	0.667	-
$d$	0.667	-
$y$	4	-
$\lambda_{G1,max}$	0.8	-
$G_2$	240	$\text{Mbar}^{-z} \mu\text{s}^{-1}$
$e$	0.667	-
$g$	0.667	-
$z$	1	-
$\lambda_{G1,max}$	0.8	-

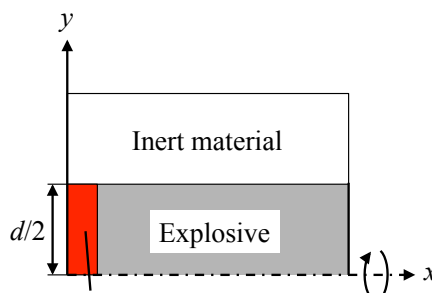
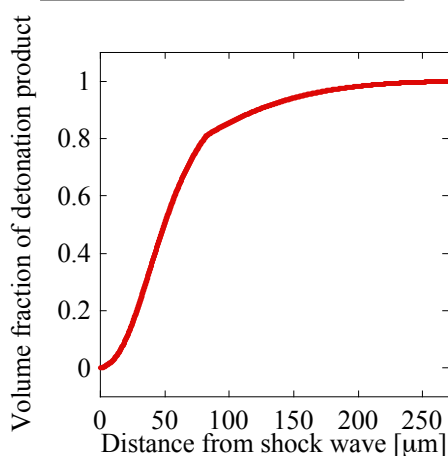


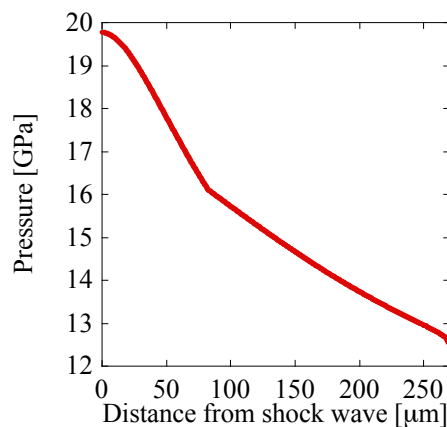
Figure 1 Schematic diagram of the calculation target

Table 3 Set of explosive and inert material

Case	Explosive	Inert material
1	NM	air
2	NM	brass



(a) Volume fraction of detonation product



(b) pressure

Figure 2 Results of 1D steady analysis of CJ detonation.

### 3 Results

In the present paper, data of the detonation with NM surrounded by the air is used to describe flow patterns. Figure 3 shows the instantaneous pictures and denotes the pressure (upper) and mass fraction of detonation products (lower) in the case of (a)  $d = 15$  mm and (b)  $d = 30$  mm. White dashed lines denote the initial interface between the NM and air. Radial flow makes curved detonation front, and the post-shock flow divergence weakens the shock wave. The unreacted region appears around the interface. In the case of 15 mm, detonation cannot maintain its propagation. After ignition ( $0 \mu\text{s}$ ), expansion wave from the interface of the explosive and the air spreads. Chemical reaction is inhibited from the interface to the axis, and detonation fails. In the case of 30 mm, the detonation maintains its propagation as shown in Fig. 3b without the change of the flow patterns such as the shock front shape and the detonation velocity.

Figure 4 shows the diameter effect for NM surrounded by air and brass. Plots and lines denote the numerical data and fitted curve proposed by Campbell and Engelke [1] with the experimental data [13]. Detonation velocities are normalized with respect to those in the case of  $1/d \sim 0$ . Our study correctly estimates the relation between the detonation velocity and diameter. Table 4 shows the critical diameter of the numerical and experimental data. Critical diameters of the numerical data agree with those of the experimental data within 10 %.

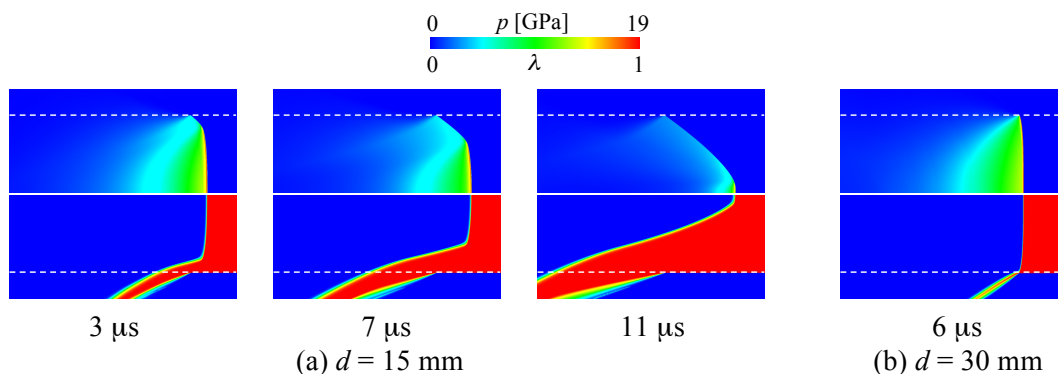
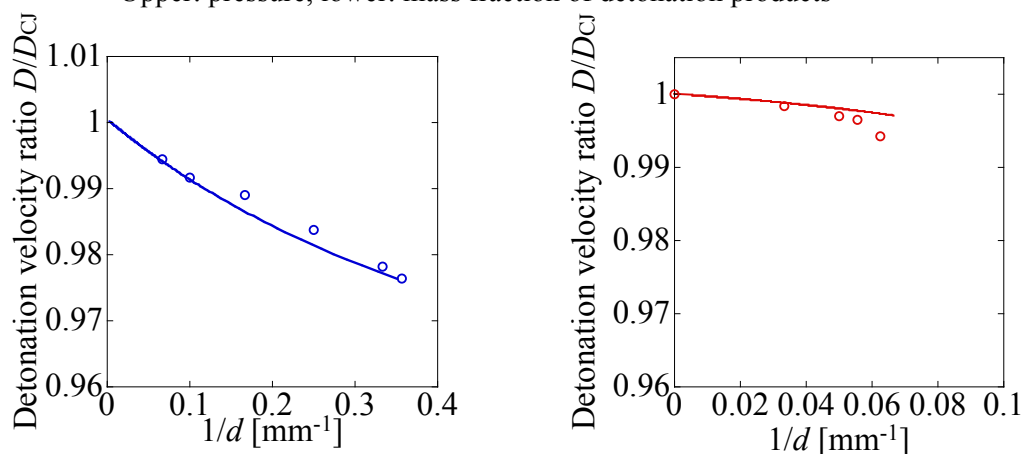


Figure 3 Instantaneous pictures of (a)  $d = 15$  mm and (b)  $d = 30$  mm.

Upper: pressure, lower: mass fraction of detonation products



(a) Nitromethane confined by heavy confinement (a) Nitromethane confined by light confinement  
Figure 4 Diameter effect. Plots; the present numerical data, lines; fitted curve [1, 14]

Table 4 Critical diameters of the experimental [12], [15] and numerical data.

confinement	Exp.	Num.
weak	$16.85 \pm 2.6$	15 - 16
strong	$2.82 \pm 0.42$	2.7 - 2.8

## 4 Conclusion

The single-pressure and single-velocity multi-phase model is used to simulate the detonation propagation of NM surrounded by air and brass. 1D steady analysis gives that CJ detonation velocity and CJ pressure agree well with the previous numerical data. the Expansion wave from the interface of the explosive and a surrounding material weakens the detonation wave, which causes inhibition of the chemical reaction and detonation failure. Our model can estimate the diameter effect of NM.

## References

- [1] Campbell AW, Engelke R. (1976). The diameter effect in high-density heterogeneous explosives. Proceedings of Sixth Symposium (International) on Detonation: 642.
- [2] Petitpas F et al. (2009). Modelling detonation waves in condensed energetic materials: multiphase CJ conditions and multidimensional computations. *Shock Waves* 19:377
- [3] Schoch S et al. (2013). Multi-phase simulation of ammonium nitrate emulsion detonations. *Combust. Flame* 160:1883
- [4] Toro EF, Spruce M, Speares W. (1994). Restoration of the contact surface in the HLL-Riemann solver. *Shock Waves* 4: 25
- [5] Zhang X, Shu C-W. (2011). Maximum-principle-satisfying and positivity-preserving high-order schemes for conservation laws: survey and new developments. *Proc. R. Soc. A* 467: 2752
- [6] Shu C-W, Osher S. (1998). Efficient implementation of essentially non-oscillatory shock-capturing schemes. *J. Comput. Phys.* 77: 439
- [7] Saurel R., Lemetayer O. (2001). A multiphase model for compressible flows with interfaces, shocks, detonation waves and cavitation. *J. Fluid Mech.* 431: 239
- [8] Fickett W, Davis WC. (1979). *Detonation: Theory and Experiment*. DOVER PUBLICATIONS, INC. (ISBN 0-486-41456-6)
- [9] Banks JW et al. (2008). A study of detonation propagation and diffraction with compliant confinement, *Combust. Theory and Modelling* 12: 769
- [10] Kapila AK et al. (2007). A study of detonation diffraction in the ignition-and-growth model, *Combust. Theory and Modelling* 11: 781
- [11] Tarver CM, Urtiew PA. (2010). Theory and modeling of liquid explosive detonation. *J Energetic Materials* 28: 299
- [12] Lee EL, Tarver CM. (1980). Phenomenological model of shock initiation in heterogeneous explosives. *Phys. Fluids* 23: 2362
- [13] Salmond J, Nikiforakis N. (2014). Characterisation of reaction waves in the initiation of detonation. 15<sup>th</sup> International Detonation Symposium, San Francisco, CA
- [14] Souers PC. (1998). A library of prompt detonation reaction zone data. Lawrence Livermore National Laboratory Report, UCRL-ID-130055 Rev 1.
- [15] Tarver CM, Shaw R, Cowperthwaite M. (1976). Detonation failure diameter studies of four liquid nitroalkanes. *The Journal of Chemical Physics* 64: 2665